Soft Matter

PAPER

Cite this: *Soft Matter*, 2017, **13**, 5905

Topological vacancies in spherical crystals

Zhenwei Yao

Received 8th August 2017,
Accepted 20th August 2017

DOI: 10.1039/c7sm01599b

rsc.li/soft-matter-journal

Understanding geometric frustration of ordered phases in two-dimensional condensed matter on curved surfaces is closely related to a host of scientific problems in condensed matter physics and materials science. Here, we show how two-dimensional Lennard-Jones crystal clusters confined on a sphere resolve geometric frustration and form pentagonal vacancy structures. These vacancies, originating from the combination of curvature and physical interaction, are found to be topological defects and they can be further classified into dislocational and disclinational types. We analyze the dual role of these crystallographic defects as both vacancies and topological defects, illustrate their formation mechanism, and present the phase diagram. The revealed dual role of the topological vacancies may find applications in the fabrication of robust nanopores. This work also shows the promising potential of exploiting richness in both physical interactions and substrate geometries to create new types of crystallographic defects, which have strong connections with the design of crystalline materials.

1 Introduction

Geometric frustration of ordered phases in two-dimensional condensed matter like crystals and liquid crystals confined on curved surfaces can create a myriad of emergent static[1–4] and dynamic[5–8] defect structures. Through the Thomson problem of finding the ground state of electrically charged particles confined on a sphere[9–13] and the generalized versions on typical curved surfaces,[4,14] several defect motifs in crystalline order like isolated disclinations, dislocations, scars and pleats have been identified in the past decades.[15–19] As a fundamental topological defect in crystalline order, a disclination refers to a vertex whose coordination number n is deviated from six in a two-dimensional triangular lattice, and a topological charge of $q = 6 - n$ can be assigned to an n-fold disclination.[1] A dislocation is a topological dipole composed of a pair of oppositely charged fivefold and sevenfold disclinations. Scars and pleats are strings of fivefold and sevenfold disclinations.[2,15,20] These frustration-induced defects are highly involved in many important physical processes like 2D crystal melting,[21–24] crystalline packings of twisted filament bundles,[25–29] self-healing of crystalline order,[7,30] non-equilibrium behaviors in active matter,[6,8,31,32] and materials design.[33–38] In a recent study, by creating depletion-induced attraction between colloidal particles confined in the interior surfaces of spherical water-in-oil droplets, vacancies were observed to proliferate in the resulting spherical crystals.[39] While the disclination structure in spherical crystals has been extensively studied theoretically and experimentally,[1,4,37,40–42] vacancies are generally unstable in spherical crystals where particles interact by the long-range Coulomb potential.[12,13] The discovery of stable vacancies as a new defect motif in curved crystals composed of attractive colloidal particles raises a number of important questions, such as what is their topological nature, the mechanism behind their formation, and their connection with the fundamental topological defects of disclinations and dislocations?

A model system suitable to address all these questions is to consider a collection of point particles confined on a sphere interacting *via* the Lennard-Jones (L-J) potential. The combination of depletion-induced short-range attraction and hard-core repulsion between colloidal particles seems to be responsible for the experimentally observed vacancies in the rigid, two-dimensional colloidal crystals on spherical droplets.[39] The L-J potential possesses both attractive and repulsive components and is a suitable form of interaction potential to study the physics of vacancies. The formally simple L-J potential has also been extensively used to model various chemical and physical bonds.[43] To lower the energy, the L-J particles on a sphere are expected to spontaneously form geometrically frustrated crystal clusters. We resorted to numerical simulations in combination with analytical theory to track the frustration of these spherical crystals and analyze the resulting defect structures therein. To highlight the geometric effect and avoid mixing the curvature driven stress and the stress due to the area constraint, we focused on particle clusters that were not fully occupying the sphere and were under stress free boundary conditions.[44] Note that the model of the L-J spherical crystal has been previously employed to study underlying physics in several aspects of shell assembly like line tension, hole implosion and closure catastrophe, where vacancy structure has been reported but its topological property is still to be clarified.[45]

School of Physics and Astronomy, and Institute of Natural Sciences, Shanghai Jiao Tong University, Shanghai 200240, China. E-mail: zyao@sjtu.edu.cn

In this work, we reveal the proliferation of pentagonal vacancies in a spherical crystal with the accumulation of the curvature effect, which are absent in planar crystals. According to their topological nature, the pentagonal vacancies can be classified into two categories: type I dislocational and type II disclinational vacancies. These two types of vacancies are topologically equivalent to 5-7 disclination pairs and 5-7-5 disclination strings, respectively. Remarkably, both vacancies exhibit identical pentagonal morphologies despite their distinct topological properties. Simulations show that their emergence is controlled by the coverage ratio of the crystal cluster over the spherical substrate. Geometric and elastic analysis shows the compatibility of the pentagonal vacancies with spherical geometry. The revealed dual role of these crystallographic defects as both vacancies and topological defects may be exploited in the fabrication of nanopore structures in crystalline membranes.[46,47] This work also shows the promising possibility of using the combination of physical interaction and geometry to create rich types of defects that may find applications in the design of crystalline materials.

2 Model

In our model, the particles confined on the sphere of radius R_0 interact *via* the L-J potential $V(r) = 4\varepsilon_0[(\sigma_0/r)^{12} - (\sigma_0/r)^6]$. The balance distance $r_m = 2^{1/6}\sigma_0$. The initial configuration of the spherical crystal cluster is prepared in the following way. We first place a line of evenly distributed M particles on the equator of the sphere, and then pile particles layer by layer along the lines of latitude separated by a distance of $\sqrt{3}r_m/2$ to fabricate a hexagonal crystal cluster. The total number of particles in the constructed spherical cluster is $N = \frac{1}{4}(3M^2 + 1)$. The initial configuration is free of stress in the limit of $R_0 \to \infty$. We employ the force method in simulations to track the evolution of the prepared crystal cluster towards the lowest-energy state.[48–50] We first calculate the force on each particle by all the other particles, and then simultaneously move all the particles by a small distance of s in each step until the energy of the system does not reduce further. Typically, $s = 10^{-4}r_m$. The system evolves towards the lowest-energy state by repeating this procedure. The underlying topological defect structures in the spherical crystals are analyzed by performing Delaunay triangulation with the software Qhull.[51] All lengths are measured in the unit of r_m. The controlling parameters are the radius of the sphere R_0 and the coverage ratio A/A_0 of the crystal cluster. A and A_0 are the areas of the crystal cluster and the sphere, respectively. Note that, in general, a condensed matter system composed of many interacting particles can be easily trapped in a metastable state.[29,52] Furthermore, due to the constraint imposed by the initial configuration of the fixed hexagonal lattice, there is a high probability that the resulting lowest-energy particle configurations found in our simulations are not the true ground states. However, it was observed that the defect structures identified in the evolution of the crystal clusters can facilitate the reduction of energy. It is therefore expected that the revealed topological vacancies can characterize the basic defect state in the true ground state.

3 Results and discussion

Fig. 1 shows the configurations of particles mapped to the $\{\theta,\phi\}$ plane, where θ and ϕ are the polar and azimuthal angles in the spherical coordinates. $\theta \in [0,\pi]$. $\phi \in [0,2\pi]$. The stretching and compression of the bonds are indicated by the red and blue lines, and more transparent bonds assume less stress. A planar crystal can wrap a developable surface of zero Gaussian curvature *via* pure bending without introducing any in-plane stress.[53] However, the geometric incompatibility between a planar crystal and a spherical substrate leads to the coupling of bending and in-plane strain.[54,55] In other words, the originally planar crystal must modify its metric by adjusting the bond length when it bends to fit the spherical geometry. The distribution of the in-plane stress in the defect free configuration at $A/A_0 = 0.08$ is shown in Fig. 1(a). The basic feature of the stress field is that the interior part of the crystal is azimuthally stretched (the hoop stress $\sigma_{\theta\theta} > 0$ for $r < r_c$), the exterior part is azimuthally compressed ($\sigma_{\theta\theta} < 0$ for $r > r_c$), and the crystal is radially stretched everywhere (the radial stress $\sigma_{rr} > 0$).

To understand the numerically observed stress pattern on the defect free spherical crystal, as shown in Fig. 1(a), we consider the elastic deformation of the originally planar crystal. The two-dimensional crystal cluster can be modelled as an isotropic elastic sheet whose elastic properties are characterized by the

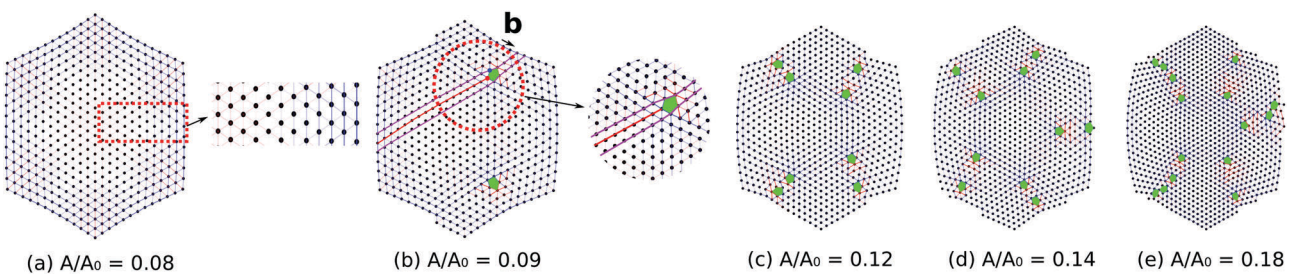

Fig. 1 Proliferation of pentagonal vacancies (in green) in a crystal cluster on a sphere with accumulation of the curvature effect. The stress pattern indicated by colored bonds (red for stretching and blue for compression) is consistent with analytical elasticity theory (see text for more information). The plots are in the plane of the spherical coordinates $\{\theta,\phi\}$. In each case, the coverage ratio of the crystal cluster A/A_0 is fixed. The inset in (b) is to illustrate the dislocational nature of the vacancy. $R_0 = 20$.

Young's modulus Y and the bending rigidity B. The ratio $t = \sqrt{B/Y}$ is the effective thickness of the sheet. For simplicity, we consider a circular elastic sheet of radius r_0. $r_0 \ll R_0$ and $r_0 \gg t$, so the stretching energy of the sheet dominates over the bending energy in the deformation.[28,41] Therefore, it is sufficient to analyze the stress state over a planar elastic sheet. The effect of the spherical substrate is to impose a normal force per area P over the elastic sheet and to pull the sheet on its edge by the force F_T per unit length to deform the sheet. The distribution of the in-plane stress is governed by the force balance equations. With the boundary conditions of $\sigma_{rr}(r = 0) = \sigma_{\theta\theta}(r = 0)$ and $\sigma_{rr}(r = r_0) = F_T$, one can derive analytical expressions for the in-plane stress field:[56] $\sigma_{\theta\theta}(r)/F_T = \beta(1 - 3(r/r_0)^2)/16 + 1$ and $\sigma_{rr}(r)/F_T = \beta(1 - (r/r_0)^2)/16 + 1$. The in-plane stress pattern is completely controlled by the parameter $\beta = (r_0/R_0)^2(Y/F_T)$. The sheet is under pure tension for $\beta < 8$. For $\beta > 8$, the hoop stress $\sigma_{\theta\theta}$ becomes compressive at the annulus $r \in \left(r_0\sqrt{(1 + 16\beta^{-1})/3},\ r_0\right)$. The coexistence of positive and negative $\sigma_{\theta\theta}$ regions in the spherical crystal in Fig. 1(a) indicates that it falls in the regime of $\beta > 8$.

For larger spherical crystal clusters, we observe the proliferation of vacancies as shown in Fig. 1(b)–(e). A vacancy in the triangular lattice can be identified where the local particle density is significantly lower than the surrounding lattice. Remarkably, we notice that these vacancies are pentagonal, which is different from the hexagonal vacancies in two-dimensional planar L-J crystals.[57] Geometric analysis reveals the dislocational nature of these pentagonal vacancies. The inset of Fig. 1(b) illustrates the extra (red) line of particles terminated at the vacancy. Integration of the resulting displacement field along any contour enclosing the vacancy returns the constant Burgers vector $\vec{b}$ that characterizes the dislocational nature of the pentagonal vacancy.[53] Delaunay triangulations show the dislocational nature of the vacancies in Fig. 1(b); they can be represented by a pair of fivefold [the red dot on the circled green pentagon in Fig. 1(b)] and sevenfold [the blue dot] disclinations. Here, we note that in the spherical crystals formed by long-range repulsive particles, vacancies and interstitials are attracted and repelled by fivefold disclinations, respectively.[12] Consequently, both vacancies and interstitials typically break up when subjected to interactions with multiple disclinations. These defects are therefore generally unstable, and have never been found in equilibrium spherical crystals where particles interact by the long-range Coulomb potential.[13]

Comparison of the configurations in Fig. 1(a) and (b) shows that the pentagonal vacancies initially appear at the interface of the compression and stretching zones. To account for these preferred sites for the emergent defects, we examine the stress field of an isolated dislocation in a two-dimensional isotropic elastic medium. In polar coordinates, we have the stress field around an isolated dislocation:[53]

$$\sigma_{rr} = \sigma_{\theta\theta} = -\frac{bB\sin\theta}{r} \quad (1)$$

and

$$\sigma_{r\theta} = \frac{bB\cos\theta}{r}, \quad (2)$$

where $B = \mu/2\pi(1 - \nu)$, μ is the shear modulus, ν is the Poisson's ratio, and b is the magnitude of the Burgers vector. θ is measured with respect to the direction of the Burgers vector. From eqn (1), we see that both radial and hoop bonds are stretched for $\theta \in (0,\pi)$ and compressed for $\theta \in (\pi,2\pi)$. Our simulations reveal stretched red bonds and compressed blue bonds around the vacancy in the inset of Fig. 1(b). Such a stress pattern is consistent with the above elastic analysis based on the assumption of a continuum elastic medium. The superposition of this stress field on the stress pattern in Fig. 1(a) can release both the compression in the exterior region [$\theta \in (0,\pi)$] and the stretching in the interior region [$\theta \in (\pi,2\pi)$]. Therefore, the pentagonal vacancies prefer to emerge at the interface of the compression and stretching zones to release the elastic energy.

With increasing coverage ratio A/A_0, Fig. 1(c)–(e) show that the spherical crystal is plagued with more dislocational pentagonal vacancies. The arrangement of these defects seems to follow a pattern. The distribution of the defects qualitatively conforms to p-fold rotational symmetry. The value for p increases from 2 (at $A/A_0 = 0.09$) to 5 (at $A/A_0 = 0.18$). Note that similar symmetric patterns of boundary defect strings as well as their broken-symmetry states in the form of forked-scar morphologies have been found in crystalline spherical caps under external tension by the combination of "free dislocation" simulations and continuum elasticity theory.[41] The internal dislocational defects in Fig. 1 also leave their signature in the exterior morphology of the crystal cluster; we will show later that the steps on the contour of the crystal cluster originate from the internal dislocations. In Fig. 1(e), we notice the unevenly distributed vacancies at the same defect string. The equally placed dislocations constitute a grain boundary to separate crystallites of distinct crystalline orientations.[52] Here, the spatial gradient in the density of dislocational vacancies will lead to net topological charges according to the elasticity theory of topological defects.[1] Furthermore, the observed inhomogeneity in the arrangement of defects in Fig. 1(e) implies the appearance of disclinational defects at even higher coverage ratios.

Further increasing the coverage ratio leads to more pentagonal vacancies, as shown in Fig. 2, for $A/A_0 = 0.50$. These vacancies can be classified by their associated topological charge. Through Delaunay triangulation, we identify a new type of pentagonal vacancy carrying positive topological charge. Such a vacancy is of disclinational nature, and is fundamentally different from the previously discussed dislocational vacancy. In Fig. 2, the two types of vacancies are indicated with different colors: dislocational vacancies by green pentagons, and disclinational ones by purple pentagons. The distinct nature of the pentagonal vacancies can also be characterized by the deformation of the lattice lines. In the inset of Fig. 2, we illustrate that lines 1 and 2 are still in parallel after passing a type I dislocational vacancy; their separation is increased by a Burgers vector's length. In contrast, the originally parallel lattice lines 3 and 4 are observed to bend and converge when passing a type II disclinational vacancy, which resembles the convergence of light rays through a convex mirror.[15,58]

We propose a geometric argument based on the Gauss–Bonnet theorem to show that the bending of the lattice lines around a

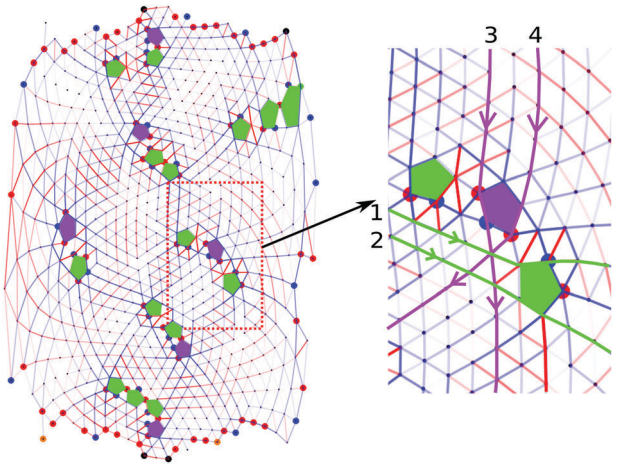

Fig. 2 Characterization of dislocational (green) and disclinational (purple) vacancies with identical pentagonal morphology. The colored bonds indicate the stretching (red) and compression (blue) patterns; strain is smaller on more transparent bonds. The plot is in the plane of the spherical coordinates $\{\theta,\phi\}$. $A/A_0 = 0.5$; $R_0 = 10$.

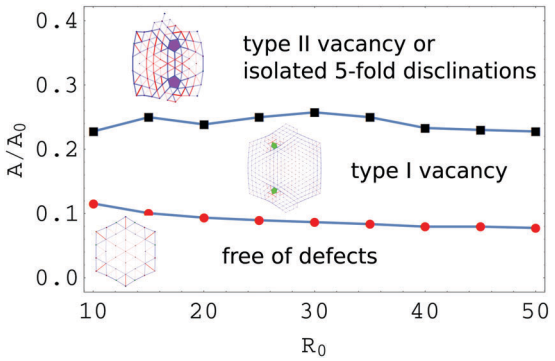

Fig. 3 Phase diagram of the defect state in L-J spherical crystals in the parameter space spanned by the coverage ratio A/A_0 and the radius R_0 of the sphere. The emergence of type I dislocational and type II disclinational vacancies is critically controlled by the coverage ratio of the crystal cluster over the sphere.

type II vacancy is compatible with the underlying spherical geometry.[54] For a compact two-dimensional Riemannian manifold M with boundary ∂M, the Gauss–Bonnet theorem states that $\int_M K_G dA + \int_{\partial M} k_g ds = 2\pi\chi(M)$, where K_G is the Gaussian curvature, k_g is the geodesic curvature, and $\chi(M)$ is the Euler characteristic of the manifold M. Applying the Gauss–Bonnet theorem to a geodesic triangle $\Delta_{g.t.}$ formed by three geodesics on the sphere, we obtain an elegant expression that connects the total curvature with the three angles:[54]

$$\int_{\Delta_{g.t.}} K_G dA = \sum_{i=1}^{3} \theta_i - \pi, \quad (3)$$

where the integration is over the geodesic triangle. It is straightforward to check that the total curvature of a planar triangle is zero.

Now let us consider a region enclosed by two converging geodesics over the sphere. Bidirectional extension of two originally parallel geodesics on the sphere will finally cause them to converge to form an eye-like shape. This region can be divided into two geodesic triangles. From eqn (3), we obtain the total curvature

$$\int K_G dA = \alpha_1 + \alpha_2, \quad (4)$$

where α_1 and α_2 are the angles at the two tips of the eye-like region. The total curvature is smaller when the eye-like shape becomes sharper. The limiting case is two parallel straight lines in a plane where the total curvature vanishes. The convergence of the approximately geodesic lines 3 and 4 in the inset of Fig. 2 is therefore compatible with the positive Gaussian curvature. Note that the convergence of lattice lines through a type II vacancy is also seen in Volterra construction for disclinations.[52] Specifically, a positive (or negative) disclinational defect in a two-dimensional triangular lattice can be constructed by removing (or inserting) a wedge of angle $\pi/3$; this operation leads to the convergence (or divergence) of originally parallel lines over a planar disk.[15]

In Fig. 3, we present the phase diagram in the parameter space of the coverage ratio A/A_0 and radius R_0 of the sphere. It clearly shows that the defect state of the spherical crystal is largely controlled by the coverage ratio, and almost unaffected by the radius of the sphere. Type I dislocational vacancies first emerge when A/A_0 exceeds about 0.1. With increasing coverage ratio, we observe the nucleation of isolated dislocational vacancies into regularly arranged strings, as shown in Fig. 1. In addition, branched defect strings as well as cracks are also numerically observed in some cases. Cracks along these vacancy strings occur in the limit of vanishingly small separation between vacancies. Fig. 3 shows that a further increase of the coverage ratio above about 0.2 leads to the proliferation of type II pentagonal vacancies or isolated fivefold disclinations within the crystal cluster. Here, it is of interest to note that, in the crystalline packings of twisted filament bundles, the emergence of dislocations and disclinations in cross-sectional crystalline order of the bundles follows a similar phase diagram in the regime of large bundles, where the appearance of these defects is critically controlled by accumulation of the curvature effect.[28]

We proceed to discuss the microscopic process in the formation of the pentagonal vacancies. In Fig. 4, we present typical snapshots at different time frames labelled by f_n in the evolution of the crystal cluster with fixed coverage ratio towards the lowest-energy state. Here, a snapshot at "time frame" f_n refers to the particle configuration obtained after n simulation steps in the evolution of our system by the rule prescribed in the Model section. In the upper snapshots in Fig. 4, we show that the formation of type I vacancies is associated with the collective movement of particles in the yellow shadow. This process can also be characterized in terms of the glide of the dislocations. The lower snapshots in Fig. 4 demonstrate the formation of type II vacancies. At $f_n = 80$, a pair of neutral linear defect strings appear with the bending of the colored lattice lines. With the extension of the red lattice line and further bending of the blue lattice line, the sevenfold disclination originally sitting at the blue line vanishes at the boundary and a pair of disclinational vacancies emerge at $f_n = 320$.

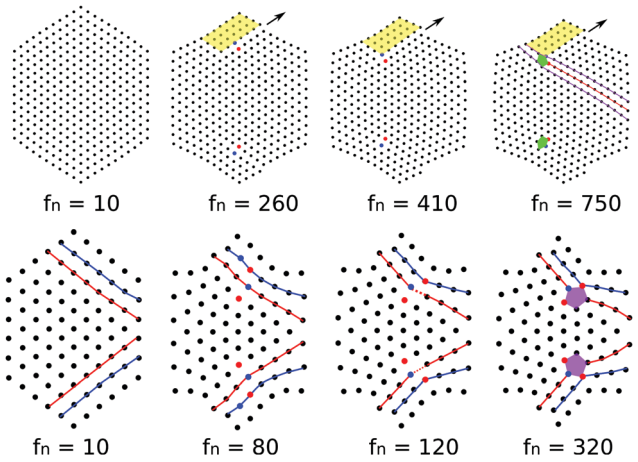

Fig. 4 Illustration of the distinct formation mechanisms of the dislocational and disclinational vacancies by tracking the evolution of the spherical crystal cluster towards the lowest-energy state. f_n is the time frame. The green and purple pentagons represent the resulting dislocational and disclinational vacancies. Upper figures: $A/A_0 = 0.1$; $R_0 = 15$. Lower figures: $A/A_0 = 0.25$; $R_0 = 5$.

We finally briefly discuss which feature in the L-J potential is responsible for the formation of the vacancies. Is it the local minimum structure or the steepness of the physical potential? While the former feature is obviously responsible for the condensation of particles to form a crystal, it is unknown if it also promotes the emergent vacancies. To answer this question, we change the 12-6 potential to the 4-2 potential $V_{4\text{-}2}(r) = 4\varepsilon_0[(\sigma_0/r)^4 - (\sigma_0/r)^2]$. The $V_{4\text{-}2}(r)$ potential also possesses a local minimum structure, but with a much softer "ductility" than the 12-6 potential. Specifically, the curvature of the 12-6 potential curve at its equilibrium position is about 14 times that of the 4-2 potential curve. By repeating the simulations leading to the configurations in Fig. 1, we find that the vacancy structures vanish. Instead, dislocations and disclinations appear to resolve the geometric frustrations. Therefore, it is the steepness of the physical potential that is responsible for the formation of the vacancy structures.

In the formation of the pentagonal vacancies in the spherical crystals, the featured sufficiently steep energy minimum in the L-J potential curve can establish a bond structure between neighboring particles, and therefore support vacancies in both planar and curved crystals.[39,57] In simulations, we extend the substrate geometry to hyperbolic paraboloid, whose Gaussian curvature is negative. By confining L-J crystal clusters on such negatively curved surfaces, we numerically observe heptagonal vacancies as well as sevenfold disclinations, as shown in Fig. 5. We also notice the negative-curvature driven coalescence of vacancies as shown in the region below the lower green box in Fig. 5. This phenomenon suggests that the model system of a negatively curved two-dimensional L-J crystal may be used to explore the mechanism of crack formation. In contrast, under purely repulsive potentials, vacancies created by removing particles were observed to be filled by neighboring particles to form dislocations.[59] Note that in our study, we focus on

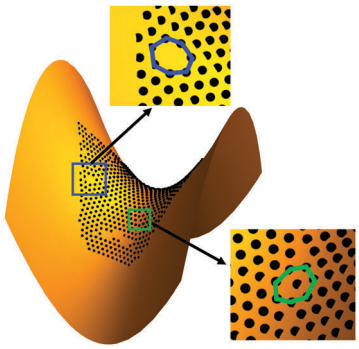

Fig. 5 Emergence of heptagonal vacancies (blue heptagon in the upper inset) and sevenfold disclinations (green heptagon in the lower inset) by confining a planar crystal cluster on the negatively curved hyperbolic paraboloid $z = (x^2 - y^2)/16$. The negative-curvature driven coalescence of vacancies is also seen in the region below the lower green box. $N = 721$.

behaviors of vacancies at zero temperature and under stress free boundary conditions, where the particle density is largely determined by the balance distance in the L-J potential. The robustness of vacancies with the variation of both particle density (*via* imposing stress on the boundary of a crystal cluster) and temperature has been shown in our previous study of planar L-J crystals, although the mobility of vacancies can be quantitatively affected by particle density and temperature.[57] While it is of interest to investigate the influence of temperature and particle density on the behaviors of topological vacancies, this is beyond the scope of this study.

4 Conclusion

In summary, we studied the geometric frustration of Lennard-Jones spherical crystals, and identified pentagonal vacancies of dislocational or disclinational nature. The transition from dislocational to disclinational vacancies is largely controlled by the coverage ratio of the crystal cluster. Clarification of the topological nature of the pentagonal vacancies in this work enhances our understanding of basic defect structures in crystalline order on curved surfaces. This work also shows the promising potential of exploiting richness in both physical interactions and substrate geometries to create new types of crystallographic defects. These defects may find applications in the design of crystalline materials, notably in the fabrication of robust polygonal nanopores on vesicles of spherical topology.

Conflicts of interest

There are no conflicts to declare.

Acknowledgements

This work was supported by NSFC Grant No. 16Z103010253, the SJTU startup fund under Grant No. WF220441904, and the award of the Chinese Thousand Talents Program for Distinguished Young Scholars under Grant No. 16Z127060004.

References

1 D. R. Nelson, *Defects and Geometry in Condensed Matter Physics*, Cambridge University Press, 2002.
2 A. Bausch, M. Bowick, A. Cacciuto, A. Dinsmore, M. Hsu, D. Nelson, M. Nikolaides, A. Travesset and D. Weitz, *Science*, 2003, **299**, 1716.
3 V. Vitelli, J. B. Lucks and D. R. Nelson, *Proc. Natl. Acad. Sci. U. S. A.*, 2006, **103**, 12323.
4 M. J. Bowick and L. Giomi, *Adv. Phys.*, 2009, **58**, 449.
5 F. C. Keber, E. Loiseau, T. Sanchez, S. J. DeCamp, L. Giomi, M. J. Bowick, M. C. Marchetti, Z. Dogic and A. R. Bausch, *Science*, 2014, **345**, 1135.
6 M. Marchetti, J. Joanny, S. Ramaswamy, T. Liverpool, J. Prost, M. Rao and R. A. Simha, *Rev. Mod. Phys.*, 2013, **85**, 1143.
7 W. T. Irvine, M. J. Bowick and P. M. Chaikin, *Nat. Mater.*, 2012, **11**, 948.
8 Z. Yao, *Soft Matter*, 2016, **12**, 7020.
9 J. J. Thomson, *Philos. Mag.*, 1904, **7**, 237.
10 E. B. Saff and A. B. J. Kuijlaars, *Math. Intell.*, 1997, **19**, 5.
11 D. J. Wales and S. Ulker, *Phys. Rev. B: Condens. Matter Mater. Phys.*, 2006, **74**, 212101.
12 M. J. Bowick, D. R. Nelson and H. Shin, *Phys. Chem. Chem. Phys.*, 2007, **9**, 6304.
13 M. Bowick, H. Shin and A. Travesset, *Phys. Rev. E: Stat., Nonlinear, Soft Matter Phys.*, 2007, **75**, 021404.
14 V. Koning and V. Vitelli, *Crystals and liquid crystals confined to curved geometries*, John Wiley & Sons, Inc, 2016.
15 W. T. Irvine, V. Vitelli and P. M. Chaikin, *Nature*, 2010, **468**, 947.
16 M. J. Bowick and Z. Yao, *Europhys. Lett.*, 2011, **93**, 36001.
17 H. Kusumaatmaja and D. J. Wales, *Phys. Rev. Lett.*, 2013, **110**, 165502.
18 D. Mehta, J. Chen, D. Z. Chen, H. Kusumaatmaja and D. J. Wales, *Phys. Rev. Lett.*, 2016, **117**, 028301.
19 C. P. Kelleher, R. E. Guerra, A. D. Hollingsworth and P. M. Chaikin, *Phys. Rev. E*, 2017, **95**, 022602.
20 M. Bowick, A. Cacciuto, D. R. Nelson and A. Travesset, *Phys. Rev. Lett.*, 2002, **89**, 185502.
21 J. M. Kosterlitz and D. J. Thouless, *J. Phys. C: Solid State Phys.*, 1973, **6**, 1181.
22 B. Halperin and D. R. Nelson, *Phys. Rev. Lett.*, 1978, **41**, 121.
23 D. R. Nelson and B. Halperin, *Phys. Rev. B: Condens. Matter Mater. Phys.*, 1979, **19**, 2457.
24 A. Radzvilavičius, *Phys. Rev. E: Stat., Nonlinear, Soft Matter Phys.*, 2012, **86**, 051111.
25 R. D. Kamien and D. R. Nelson, *Phys. Rev. Lett.*, 1995, **74**, 2499.
26 R. D. Kamien, *J. Phys. II*, 1996, **6**, 461.
27 G. M. Grason, *Phys. Rev. E: Stat., Nonlinear, Soft Matter Phys.*, 2012, **85**, 031603.
28 A. Azadi and G. M. Grason, *Phys. Rev. E: Stat., Nonlinear, Soft Matter Phys.*, 2012, **85**, 031604.
29 I. R. Bruss and G. M. Grason, *Soft Matter*, 2013, **9**, 8327.
30 Z. Yao and M. Olvera de la Cruz, *Proc. Natl. Acad. Sci. U. S. A.*, 2014, **111**, 5094.
31 B. M. Mognetti, A. Šarić, S. Angioletti-Uberti, A. Cacciuto, C. Valeriani and D. Frenkel, *Phys. Rev. Lett.*, 2013, **111**, 245702.
32 J. Palacci, S. Sacanna, A. P. Steinberg, D. J. Pine and P. M. Chaikin, *Science*, 2013, **339**, 936.
33 D. R. Nelson, *Nano Lett.*, 2002, **2**, 1125.
34 G. A. DeVries, M. Brunnbauer, Y. Hu, A. M. Jackson, B. Long, B. T. Neltner, O. Uzun, B. H. Wunsch and F. Stellacci, *Science*, 2007, **315**, 358.
35 M. Brojan, D. Terwagne, R. Lagrange and P. M. Reis, *Proc. Natl. Acad. Sci. U. S. A.*, 2015, **112**, 14.
36 T. Zhang, X. Li and H. Gao, *J. Mech. Phys. Solids*, 2014, **67**, 2.
37 D. J. Wales, *ACS Nano*, 2014, **8**, 1081.
38 F. L. Jiménez, N. Stoop, R. Lagrange, J. Dunkel and P. M. Reis, *Phys. Rev. Lett.*, 2016, **116**, 104301.
39 G. Meng, J. Paulose, D. R. Nelson and V. N. Manoharan, *Science*, 2014, **343**, 634.
40 Y. Chushak and A. Travesset, *Europhys. Lett.*, 2005, **72**, 767.
41 A. Azadi and G. M. Grason, *Phys. Rev. Lett.*, 2014, **112**, 225502.
42 A. Azadi and G. M. Grason, *Phys. Rev. E*, 2016, **94**, 013003.
43 J. N. Israelachvili, *Intermolecular and Surface Forces*, Academic Press, 3rd edn, 2011.
44 D. Roshal, C. Y. Petrov, A. Myasnikova and S. Rochal, 2013, arXiv preprint arXiv:1309.7906.
45 A. Luque, D. Reguera, A. Morozov, J. Rudnick and R. Bruinsma, *J. Chem. Phys.*, 2012, **136**, 184507.
46 A. Dinsmore, M. F. Hsu, M. Nikolaides, M. Marquez, A. Bausch and D. Weitz, *Science*, 2002, **298**, 1006.
47 M. Dubois, B. Demé, T. Gulik-Krzywicki, J.-C. Dedieu, C. Vautrin, S. Désert, E. Perez and T. Zemb, *Nature*, 2001, **411**, 672.
48 E. Bendito, M. J. Bowick, A. Medina and Z. Yao, *Phys. Rev. E: Stat., Nonlinear, Soft Matter Phys.*, 2013, **88**, 012405.
49 Z. Yao and M. Olvera de la Cruz, *Phys. Rev. Lett.*, 2013, **111**, 115503.
50 Z. Yao and M. Olvera de la Cruz, *Phys. Rev. Lett.*, 2016, **116**, 148101.
51 C. B. Barber, D. P. Dobkin and H. Huhdanpaa, *ACM Trans. Math. Software*, 1996, **22**, 469.
52 P. Chaikin, T. Lubensky and T. Witten, *Principles of Condensed Matter Physics*, Cambridge Univ. Press, 2000.
53 L. Landau and E. Lifshitz, *Theory of Elasticity*, Butterworth, Oxford, 1999.
54 D. Struik, *Lectures on Classical Differential Geometry*, Dover Publications, 2nd edn, 1988.
55 B. Audoly and Y. Pomeau, *Elasticity and Geometry*, Oxford Univ. Press, 2010.
56 G. M. Grason and B. Davidovitch, *Proc. Natl. Acad. Sci. U. S. A.*, 2013, **110**, 12893.
57 Z. Yao and M. Olvera de la Cruz, *Phys. Rev. E: Stat., Nonlinear, Soft Matter Phys.*, 2014, **90**, 062318.
58 R. D. Kamien, D. R. Nelson, C. D. Santangelo and V. Vitelli, *Phys. Rev. E: Stat., Nonlinear, Soft Matter Phys.*, 2009, **80**, 051703.
59 A. Pertsinidis and X. Ling, *Nature*, 2001, **413**, 147.